IEEE Access
Multidisciplinary | Rapid Review | Open Access Journal

Received June 22, 2019, accepted July 24, 2019, date of publication July 30, 2019, date of current version August 14, 2019.

Digital Object Identifier 10.1109/ACCESS.2019.2932110

Micro Doppler Reconstruction From Discontinuous Observations Based on Gapped SBL-FBTVAR Method for Spin Stabilized Object

LING HONG[1,2], FENGZHOU DAI[3], AND XILI WANG[1,2]

[1]Key Laboratory of Modern Teaching Technology, Ministry of Education, Shaanxi Normal University, Shaanxi 710119, China
[2]School of Computer Science, Shaanxi Normal University, Shaanxi 710119, China
[3]Key Laboratory of Radar Signal Processing, Xidian University, Shannxi 710071, China

Corresponding authors: Fengzhou Dai (fzdai@xidian.edu.cn) and Xili Wang (learning527@126.com)

This work was supported in part by the National Natural Science Foundation of China under Grant 61701290 and Grant 41471280, in part by the Natural Science Basic Research Plan in Shaanxi Province of China under Grant 2018JQ6052, in part by the China Postdoctoral Science Foundation under Grant 2016M592747, and in part by the Postdoctoral Science Foundation in Shaanxi Province of China under Grant 2017BSHEDZZ83.

ABSTRACT Micro Doppler analysis of spin stabilized objects is of a great significance for attitude estimation and recognition of space targets. In practice, the radar cannot dwell on one target in a long interval continuously. In this paper, we propose a novel approach for the micro Doppler frequency recovery from the discontinuous radar observations, which is referred to as gapped sparse Bayesian learning forward backward time-varying autoregressive (GSBL-FBTVAR) method. First, the sparse optimization model for estimating the sparse FBTVAR model coefficients from gapped samples is established. Then, the sparse FBTVAR model parameters corresponding to the gapped sampled data and the missing data are estimated via an extended sparse Bayesian learning (SBL) algorithm and the missing-data iterative adaptive approach (MIAA). The micro Doppler frequencies are estimated by investigating the relationship between the model parameters and the poles. Finally, the experiments are carried out on the electromagnetic analysis data to verify the proposed GSBL-FBTVAR method.

INDEX TERMS Spin stabilized object, micro Doppler recovery, gapped samples, TVAR, sparse Bayesian learning.

I. INTRODUCTION

The spin stability is a method which is widely used in the attitude control of space objects, such as missiles and satellites [1]. In practice, since the torque caused by micro force or massive imbalance cannot be avoided completely, the nutation and precession are present accompanying with the spin for most real spin stabilized objects [1]. In the radar field, the spin, the precession and the nutation are referred to as micro motions. The micro motions will generate a nonlinear and time-varying Doppler modulation in the radar return of the object, which is called the micro Doppler effect [2]. Since the micro Doppler contains the rich information of the attitude of the object, it is significant for the object identification [2]–[6].

As a specific application of the micro Doppler, the theory and method on micro Doppler analysis and processing of spin objects draw a wide attention in the radar field [3], [4], [7]–[12]. In [3], [4], the micro Doppler of the spin stabilized ballistic missile is analyzed. In [7]–[10], the methods of 3-D spin and precession features and structure characteristics extraction of a cone-like spin target based on micro Doppler were proposed. Reference [11] proposed a method to estimate the micro motion parameters of a spin stabilized object with unknown shape. And reference [12] developed a technique to classify the warheads and the confusing objects according to the micro Doppler. In the literatures mentioned above, it is assumed that the radar observes a target continuously in an interval of several seconds to obtain the micro Doppler

The associate editor coordinating the review of this manuscript and approving it for publication was Pietro Savazzi.

of the target. However, in practice, the radar is required to track multiple targets in different beams and search in some regions in most cases, which causes that the resource of the radar cannot dwell on one target continuously in a long interval [13], [14]. Usually, the micro Doppler signal of the spin stabilized object is nonstationary, and the problem of the micro Doppler signal processing in the multiple targets tracking scenarios can be boiled down to the instantaneous frequency (IF) estimation of the nonstationary signal from the gapped or incomplete data.

For stationary signals, the problem of spectral estimation from the gapped data or incomplete data is considered thoroughly, and some effective algorithms based on the filter banks [15]–[17] and the sparse reconstruction [18] were developed. Recently, the problem of the nonstationary signal recovery has received much attention. However, most of the relative works focus on the cases of random missing samples [19]–[28], and exploit the sparsity of the signals in the time-frequency (TF) domain based on the compressive sensing (CS) technology [20]–[25]. Unlike the artifacts caused by the random missing data which are uniformly distributed in the TF plane, higher artifacts caused by the gapped missing data are concentrated around the true signals in TF domain [27], [28]. As a result, the IF estimation from the gapped sampled nonstationary signal is much more challenging.

To the best of our knowledge, the work addressing the TF analysis for the nonstationary signal with the gapped missing data is much less than that of the TF analysis with random missing data. By exploiting the Fourier transform relationship between the Wigner-Ville distribution (WVD) and the instantaneous ambiguity function (IAF) and the sparsity of the signal in the TF plane, a method based on the missing-data iterative adaptive approach (MIAA) in the IAF is proposed in [27] to handle the problem of IF estimation form gapped sampled data. In the latest work [28], a more efficient method based on CS in the IAF is proposed, and the adaptive optimal kernel is integrated to suppress the cross terms of multiple components. The method is referred to as missing data iterative sparse reconstruction with adaptive optimal kernel, MI-SR (AOK).

In this paper, we develop a novel gapped sparse Bayesian learning forward backward time-varying autoregression (GSBL-FBTVAR) model to recover the micro Doppler frequencies from the gapped sampled radar return signals. The TVAR model is a parametric time-frequency method, which allows one to incorporate the prior information of the signal and to take advantages of the good time-frequency resolution and the effective noise reduction [29]–[34]. Unfortunately, the conventional least square (LS) TVAR method is not suitable to deal with the discontinuous observations. In the proposed method, the problem of the instantaneous frequency recovery from the gapped radar data is transformed to the FBTVAR model coefficients estimation problem. The coefficients of the FBTVAR model corresponding to the available samples are estimated jointly among the discontinuous sample segments by the extended sparse Bayesian learning (SBL) algorithm [35] and the coefficients corresponding to the missing samples are recovered by the missing-data iterative adaptive approach (MIAA). There are two advantages to recover the micro Doppler from discontinuous observations via the proposed method. 1) The micro Doppler of the object can be estimated from the gapped observations jointly based on an unified TVAR model with sparse constraints, which can not be solved by the LS TVAR method; 2) the proposed method avoids the micro Doppler frequencies association of multiple scatterers among the discontinuous observation segments by utilizing the relationship between the instantaneous frequencies of the nonstationary signal and the coefficients of the TVAR model.

The rest of this paper is organized as follows. In Section II, we introduce the mathematical model of the micro Doppler of a spin stabilized symmetric rigid object. In Section III, we construct the sparse optimization problem to estimate the FBTVAR coefficients from the gapped observations. In Section IV, an extended SBL algorithm is developed to solve the sparse FBTVAR problem corresponding to the available observations, and the MIAA is employed to recover the time-varying coefficients of the missing data from those of the observed data. In Section V, the performance of the proposed method is verified by a series of simulations based on the electromagnetic analysis data. And the conclusions are drawn in Section VI.

II. MICRO DOPPLER OF THE SPIN STABLIZED OBJECT

The motion of the spin stabilized space object can be decomposed into the centroid motion and the micro motion. Here, we assume that the centroid motion is completely compensated according to the orbit information. The micro motion of the spin stabilized object can be approximated by the superposition of the spin and the motion of the spin axis. The later can be further decomposed into the conical rotation of the spin axis around the nutation axis with the nutation angular frequency ω_{N} and the conical rotation of the nutation axis around the precession axis with the precession angular frequency ω_{P}. To establish the coordinates systems, the intersecting point of the spin axis, the nutation axis and the precession axis is set as the origin O. The axes aligned with the precession axis, the nutation axis and the spin axis are defined as Z of $OXYZ$, w of $Ouvw$ and z of $Oxyz$, respectively. The object-fixed coordinate system $Oxyz$ rotates with the object and the reference coordinate system $OXYZ$ is moving with the trajectory of the object. Moreover, the angle between the spin axis and the nutation axis ψ and the angle between the nutation axis and the precession axis β are constant in stable state [11]. The z axis of the object-fixed coordinate system is aligned with the spin axis of the object, and the center is on the centroid of the object. The micro motion of a symmetrical object is illustrated in Fig.1. For a symmetrical object, the dominant scatterers are the slipping scatterers coming from the edge of the object [4], [11] and only the precession and the nutation can be observed from the micro

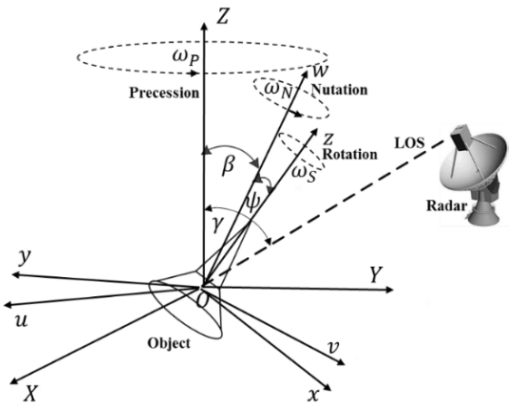

FIGURE 1. Geometry of a spin stabilized object.

Doppler signal of the slipping scatterers. Assume that the angle between the light of sight (LOS) and the precession axis is γ, and the coordinate values of the kth slipping scatterer in the object-fixed coordinate system is (x_k, z_k). According to [11], the slant range of this scatterer r_k at the time t is given by,

$$r_k(t) = \mathbf{s}_k \mathbf{c}(t)^T = x_k \sin\theta(t) + z_k \cos\theta(t) \tag{1}$$

where $\mathbf{s}_k = \begin{bmatrix} x_k & z_k \end{bmatrix}$, $\mathbf{c}(t) = \begin{bmatrix} \sin\theta(t) & \cos\theta(t) \end{bmatrix}$, the superscript "$T$" represents the operation of transpose, and $\theta(t)$ is the angle between the LOS and the spin axis and expressed as,

$$\begin{aligned}\theta(t) = \arccos\{&\sin\gamma(\sin\beta\cos\psi \\ &+ \cos\beta\sin\psi\sin(\omega_N t))\cos(\omega_P t) \\ &- \sin\gamma\sin\psi\cos(\omega_N t)\sin(\omega_P t) \\ &+ \cos\gamma[\cos\beta\cos\psi - \sin\beta\sin\psi\sin(\omega_N t)]\}\end{aligned} \tag{2}$$

The instantaneous velocity of the kth slipping scatterer is given by,

$$v_k(t) = \frac{dr_k(t)}{dt} = \left[z_k - x_k \frac{h(t)}{\sqrt{1-h^2(t)}}\right]\frac{dh(t)}{dt} \tag{3}$$

where $h(t) = \cos[\theta(t)]$ and its derivative to the time t is,

$$\begin{aligned}\frac{dh(t)}{dt} = &\omega_N \sin\gamma\cos\beta\sin\psi\cos(\omega_N t)\cos(\omega_P t) \\ &- \omega_P \sin\gamma\cos\beta\sin\psi\sin(\omega_N t)\sin(\omega_P t) \\ &- \omega_P \sin\gamma\sin\beta\cos\psi\sin(\omega_P t) \\ &+ \omega_N \sin\gamma\sin\psi\sin(\omega_N t)\sin(\omega_P t) \\ &- \omega_P \sin\gamma\sin\psi\cos(\omega_N t)\cos(\omega_P t) \\ &- \omega_N \cos\gamma\sin\beta\sin\psi\cos(\omega_N t)\end{aligned} \tag{4}$$

Substitute (2) and (4) into (3), we can obtain the instantaneous velocity of the kth slipping scatterer, and its micro Doppler frequency fd_k at the time t is given by,

$$fd_k(t) = \frac{2v_k(t)}{\lambda} \tag{5}$$

where λ is the wavelength of the radar transmitting signal.

Assume the pulse repetition interval is T_r, and there are K slipping scatterers on the object to be observed, and then the baseband signal of the target return after the range compression from the mth pulse can be expressed as,

$$s(m) = \sum_{k=1}^{K} a_k(m) \exp\left[j2\pi \int_0^{mT_r} fd_k(t)\,dt\right] \quad m = 0, \ldots, M-1 \tag{6}$$

where $a_k(m)$ is the amplitude modulation function of the kth slipping scatterer, and M is the number of the radar transmit pulses during the observation interval.

III. SPARSE TVAR MODEL OF THE GAPPED SAMPLED MICRO DOPPLER SIGNAL

Assume that the complete observation interval contains G times discontinuous dwelling of the radar beam on the target, and the signal can be modeled as G observable segments spaced with $G-1$ segments of the missing data. Then the observation of the gth segment is,

$$x_g(m) = s_g(m) + n_g(m), \quad m = 0, \cdots, M_g - 1 \tag{7}$$

where $s_g(m)$ and $n_g(m)$ are the signal and the complex white Gaussian noise of the gth segment, respectively, the form of the signal $s_g(m)$ is given by (6), and M_g is the number of the pulses of the gth segment. That is, the number of all the observations is $M = \sum_{g=1}^{G} M_g$.

The TVAR model is a method for the instantaneous frequency estimation of the nonstationary signal with high precision and good robustness to noise [29]–[31]. The P–order forward and backward TVAR model of $x_g(m)$ are of the form,

$$\begin{aligned}x_g(m) &= -\sum_{p=1}^{P} c_p(m_{m,g})\, x_g(m-p) + w(m_{m,g}) \\ &\quad m = P, \cdots, M_g - 1\end{aligned} \tag{8}$$

$$\begin{aligned}x_g(m) &= -\sum_{p=1}^{P} c_p^*(m_{m,g})\, x_g(m+p) + w(m_{m,g}) \\ &\quad m = 0, \cdots, M_g - P - 1\end{aligned} \tag{9}$$

where $m_{m,g}$ denoting the sampling instant of the mth sample of the gth sample segment, $c_p(m_{m,g})$ is the pth order time-varying coefficient at the time $m_{m,g}$, the superscripts "$*$" denotes the conjugate, $w(m_{m,g})$ denotes the complex white noise with the mean being zero and the variance being σ_w^2. Generally, it is nontrivial to directly compute the time-varying model parameters $c_p(m_{m,g})$. To convert the time-varying model parameters estimation problem to be time-invariant, $c_p(m_{m,g})$ can be expanded as a linear combination of a set of basis functions $f_q(m_{m,g})$, $q = 1, \cdots, Q$,

$$c_p(m_{m,g}) = \sum_{q=1}^{Q} b_{pq} f_q(m_{m,g}) \tag{10}$$

$$\mathbf{X}_g^f = \begin{bmatrix} f_1(m_{P,g})x_g(P-1) & \cdots & f_Q(m_{P,g})x_g(P-1) & \cdots & f_1(m_{P,g})x_g(0) & \cdots & f_Q(m_{P,g})x_g(0) \\ f_1(m_{P+1,g})x_g(P) & \cdots & f_Q(m_{P+1,g})x_g(P) & \cdots & f_1(m_{P+1,g})x_g(1) & \cdots & f_Q(m_{P+1,g})x_g(1) \\ \vdots & \ddots & \vdots & \cdots & \vdots & \ddots & \vdots \\ f_1(m_{M_g-1,g})x_g(M_g-2) & \cdots & f_Q(m_{M_g-1,g})x_g(M_g-2) & \cdots & f_1(m_{M_g-1,g})x_g(M_g-P-1) & \cdots & f_Q(m_{M_g-1,g})x_g(M_g-P-1) \end{bmatrix} \tag{15}$$

$$\mathbf{X}_g^b = \begin{bmatrix} f_1^*(m_{0,g})x_g(1) & \cdots & f_Q^*(m_{0,g})x_g(1) & \cdots & f_1^*(m_{0,g})x_g(P) & \cdots & f_Q^*(m_{0,g})x_g(P) \\ f_1^*(m_{1,g})x_g(2) & \cdots & f_Q^*(m_{1,g})x_g(2) & \cdots & f_1^*(m_{1,g})x_g(P+1) & \cdots & f_Q^*(m_{1,g})x_g(P+1) \\ \vdots & \ddots & \vdots & \cdots & \vdots & \ddots & \vdots \\ f_1^*(m_{M_g-P-1,g})x_g(M_g-P) & \cdots & f_Q^*(m_{M_g-P-1,g})x_g(M_g-P) & \cdots & f_1^*(m_{M_g-P-1,g})x_g(M_g-1) & \cdots & f_Q^*(m_{M_g-P-1,g})x_g(M_g-1) \end{bmatrix} \tag{16}$$

where Q is the number of the basis functions, b_{pq}, $p = 1, \ldots, P, q = 1, \ldots, Q$ are the time-invariant coefficients. Usually, the basis function can be the discrete cosine transform (DCT) basis, the discrete Fourier transform (DFT) basis, the Chebysheve basis, the polynomial basis, etc.

Substitute (10) into (8) and (9), and then the forward and backward TVAR models of all the G observed data segments can be rewritten in the matrix-vector form,

$$\mathbf{x}_\mathrm{f} = -\mathbf{X}_\mathrm{f}\boldsymbol{\beta} + \mathbf{w}_\mathrm{f} \tag{11}$$

$$\mathbf{x}_\mathrm{b} = -\mathbf{X}_\mathrm{b}\boldsymbol{\beta}^* + \mathbf{w}_\mathrm{b} \tag{12}$$

where $\mathbf{w_f} = [w(m_{P,g}), w(m_{P+1,g}), \cdots, w(m_{M_g-1,g})]^T$ and $\mathbf{w_b} = [w(m_{0,g}), w(m_{1,g}), \cdots, w(m_{M_g-P-1,g})]^T$ are the observation noise vectors; $\boldsymbol{\beta} = [b_{11}, b_{12}, \ldots, b_{1Q}, \ldots, b_{P1}, b_{P2}, \ldots, b_{PQ}]^T$ is the time-invariant coefficient vector of the forward TVAR model, and $\boldsymbol{\beta}^* = [b_{11}^*, b_{12}^*, \ldots, b_{1Q}^*, \ldots, b_{P1}^*, b_{P2}^*, \ldots, b_{PQ}^*]^T$ is the time-invariant parameters vector of the backward TVAR model; the forward measured data vector is $\mathbf{x}_\mathrm{f} = [\,(\mathbf{x}_1^\mathrm{f})^T\ (\mathbf{x}_2^\mathrm{f})^T \cdots (\mathbf{x}_G^\mathrm{f})^T\,]^T$ with $\mathbf{x}_g^\mathrm{f} = \left[x_g(P), x_g(P+1), \ldots, x_g(M_g-1)\right]^T$, $g = 1, \ldots, G$, and the backward measured data vector is $\mathbf{x}_\mathrm{b} = [(\mathbf{x}_1^\mathrm{b})^T\ (\mathbf{x}_2^\mathrm{b})^T \cdots (\mathbf{x}_G^\mathrm{b})^T]^T$ with $\mathbf{x}_g^\mathrm{b} = [x_g(0), x_g(1), \ldots, x_g(M_g-P-1)]^T$, $g = 1, \ldots, G$; the forward and backward partially data matrix are defined as,

$$\mathbf{X}_\mathrm{f} = \left[\,(\mathbf{X}_1^\mathrm{f})^T \quad (\mathbf{X}_2^\mathrm{f})^T \quad \cdots \quad (\mathbf{X}_G^\mathrm{f})^T\,\right]^T \tag{13}$$

$$\mathbf{X}_\mathrm{b} = \left[\,(\mathbf{X}_1^\mathrm{b})^T \quad (\mathbf{X}_2^\mathrm{b})^T \quad \cdots \quad (\mathbf{X}_G^\mathrm{b})^T\,\right]^T \tag{14}$$

where $\mathbf{X}_g^f$ and $\mathbf{X}_g^b$ are denoted in (15) and (16), respectively, as shown at the top of this page.

In the existing TVAR methods, the samples are assumed to be successive, and the time-invariant coefficient vector $\boldsymbol{\beta}$ can be estimated by the LS method as follows,

$$\hat{\boldsymbol{\beta}}_\mathrm{LS} = -\left(\mathbf{X}_\mathrm{f}^H\mathbf{X}_\mathrm{f} + \mathbf{X}_\mathrm{b1}^H\mathbf{X}_\mathrm{b1}\right)^{-1}\left(\mathbf{X}_\mathrm{f}^H\mathbf{x}_\mathrm{f} + \mathbf{X}_\mathrm{b1}^H\mathbf{x}_\mathrm{b1}\right) \tag{17}$$

where $\hat{\boldsymbol{\beta}}_\mathrm{LS}$ is the LS estimator of $\boldsymbol{\beta}$, $\mathbf{X}_\mathrm{b1} = \mathbf{X}_\mathrm{b}^*$, $\mathbf{x}_\mathrm{b1} = \mathbf{x}_\mathrm{b}^*$.

However, here $\boldsymbol{\beta}$ is not suitable to be estimated by the LS method, as the time-varying coefficients of the TVAR model are not smooth at the end points of the different segments. Considering that the number of the nonzero values of $\boldsymbol{\beta}$ is small for most nonstationary signals and the sparse optimization is successful for the signal recovery from the discontinuous samples by preventing the LS estimation from overfitting [18], we propose a sparse-aware method to estimate $\boldsymbol{\beta}$ from the gapped samples by solving the following optimization problem,

$$\begin{cases} \min\limits_{\boldsymbol{\beta}} \ \|\mathbf{x}_\mathrm{f} + \mathbf{X}_\mathrm{f}\boldsymbol{\beta}\|_2^2 + \|\mathbf{x}_\mathrm{b1} + \mathbf{X}_\mathrm{b1}\boldsymbol{\beta}\|_2^2 \\ s.t.\ \ |\boldsymbol{\beta}|_1 < \delta \end{cases} \tag{18}$$

where $|\boldsymbol{\beta}|_1 = \sum\limits_{p=1}^{P}\sum\limits_{q=1}^{Q}\left|b_{pq}\right|$ and δ is the sparsity controlling parameter.

Once $\boldsymbol{\beta}$ becomes available, it is easy to calculate the time-varying coefficients $c_p(m)$ according to (10). Then, we can compute the P poles $\rho_p(m), p = 1, \ldots, P$ as functions of time by investigating the relationship between the TVAR coefficients and the poles,

$$1 + \sum_{p=1}^{P} c_p(m)z^{-p} = \prod_{p=1}^{P}(1 - \rho_p(m)z^{-1}), \quad m \in \{\text{All instants}\} \tag{19}$$

where z is the variable of the Z-transform.

The estimation of the micro Doppler frequencies corresponding to the pth pole can be calculated as follows,

$$\hat{fd}_p(m) = \arctan\left(\frac{\mathrm{Im}\left[\rho_p(m)\right]}{\mathrm{Re}\left[\rho_p(m)\right]}\right)\Big/2\pi, \quad m \in \{\text{All instants}\} \tag{20}$$

To this end, it is obvious that the key point to estimate the micro Doppler frequencies is to calculate the time-varying model coefficients. Since the data is gapped sampled, the micro Doppler frequencies will be recovered as two parts:

one is corresponding to the observed data and the other is corresponding to the missing data.

IV. MICRO DOPPLER RECOVERY BASED ON THE GAPPED SBL-FBTVAR AND MIAA

A. THE EXTENDED SBL ALGORITHM FOR TVAR COEFFICIENTS ESTIMATION FROM THE GAPPED DATA

Among the algorithms for resolving the sparse optimization, the SBL method is robust when the sparse information of the signal is absent [35]. The available SBL method is designed for the problem with single ℓ_2 norm object function. Here the object function is the sum of two ℓ_2 norms as in (18), and thus we need to extend the available SBL algorithm to solve the problem as following, which is referred to as GSBL-FBTVAR.

Assume the time-invariant coefficient vector $\boldsymbol{\beta} \in \mathbb{C}^{PQ}$ obeys the multi-variate complex Gaussian distribution,

$$p(\boldsymbol{\beta};\boldsymbol{\gamma}) \sim \prod_{i=1}^{PQ} CN(0,\gamma_i) \tag{21}$$

where $\boldsymbol{\gamma} = [\gamma_1, \cdots, \gamma_{PQ}]$ is a $PQ \times 1$ hyperparameter vector with γ_i being the prior variance of the weight component β_i.

Suppose the observation noise is the complex white noise with zero means and $\sigma^2\mathbf{I}_{M-p}$ covariance matrix, where $\mathbf{I}_{M-p}$ is the $(M-p)$-dimensional identical matrix, i.e.,

$$p(\mathbf{w}_{\mathrm{f}};\sigma^2) \sim CN(0,\sigma^2\mathbf{I}_{M-p}) \tag{22}$$

and

$$p(\mathbf{w}_{\mathrm{b}};\sigma^2) \sim CN(0,\sigma^2\mathbf{I}_{M-p}) \tag{23}$$

According to (21) $\sim$ (23), it is easy to obtain the posterior density of $\boldsymbol{\beta}$ from $\mathbf{x}_{\mathrm{f}}$ and $\mathbf{x}_{\mathrm{b1}}$ as,

$$p(\boldsymbol{\beta}_1|\mathbf{x}_{\mathrm{f}};\sigma^2,\boldsymbol{\gamma}) \sim CN(\mu_{\boldsymbol{\beta}_1},\boldsymbol{\Sigma}_{\boldsymbol{\beta}_1}) \tag{24}$$

and

$$p(\boldsymbol{\beta}_2|\mathbf{x}_{\mathrm{b1}};\sigma^2,\boldsymbol{\gamma}) \sim CN(\mu_{\boldsymbol{\beta}_2},\boldsymbol{\Sigma}_{\boldsymbol{\beta}_2}) \tag{25}$$

where,

$$\begin{aligned}\boldsymbol{\mu}_{\boldsymbol{\beta}_1} &= \sigma^{-2}\boldsymbol{\Sigma}_{\boldsymbol{\beta}_1}\mathbf{X}_{\mathrm{f}}^H\mathbf{x}_{\mathrm{f}}\\ \boldsymbol{\Sigma}_{\boldsymbol{\beta}_1} &= (\boldsymbol{\Sigma}_0^{-1}+\sigma^{-2}\mathbf{X}_{\mathrm{f}}^H\mathbf{X}_{\mathrm{f}})^{-1}\end{aligned} \tag{26}$$

and

$$\begin{aligned}\boldsymbol{\mu}_{\boldsymbol{\beta}_2} &= \sigma^{-2}\boldsymbol{\Sigma}_{\boldsymbol{\beta}_2}\mathbf{X}_{\mathrm{b1}}^H\mathbf{x}_{\mathrm{b1}}\\ \boldsymbol{\Sigma}_{\boldsymbol{\beta}_2} &= (\boldsymbol{\Sigma}_0^{-1}+\sigma^{-2}\mathbf{X}_{\mathrm{b1}}^H\mathbf{X}_{\mathrm{b1}})^{-1}\end{aligned} \tag{27}$$

where the superscript "H" represents the conjugate transpose operations on one complex matrix or vector, and the subscript "1" and "2" correspond to the forward measured data vector $\mathbf{x}_{\mathrm{f}}$ and the backward measured data vector $\mathbf{x}_{\mathrm{b}}$, respectively, and so forth.

Then, the time-invariant coefficient vector can be chosen by satisfying,

$$\begin{aligned}\boldsymbol{\beta} &= (\boldsymbol{\beta}_1+\boldsymbol{\beta}_2)/2\\ &= (\sigma^2\boldsymbol{\Sigma}_0^{-1}+\mathbf{X}_{\mathrm{f}}^H\mathbf{X}_{\mathrm{f}})^{-1}\mathbf{x}_{\mathrm{f}}/2\\ &\quad +(\sigma^2\boldsymbol{\Sigma}_0^{-1}+\mathbf{X}_{\mathrm{b1}}^H\mathbf{X}_{\mathrm{b1}})^{-1}\mathbf{x}_{\mathrm{b1}}/2\end{aligned} \tag{28}$$

where $\boldsymbol{\Sigma}_0 \triangleq \mathrm{diag}(\boldsymbol{\gamma})$.

Thus, the key point is to estimate the parameters $\Omega = \{\boldsymbol{\gamma},\sigma^2\}$, which can be obtained by utilizing the fast expectation–maximization algorithm. The update formulas are derived as follows,

$$\begin{aligned}\gamma_{i1} &\leftarrow \left|\boldsymbol{\mu}_{\boldsymbol{\beta}_1}^i\right|^2/(1-\gamma_{i1}^{-1}\boldsymbol{\Sigma}_{\boldsymbol{\beta}_1}^{ii})\\ \sigma_1^2 &\leftarrow \left\|\mathbf{x}_{\mathrm{f}}+\mathbf{X}_{\mathrm{f}}\boldsymbol{\mu}_{\boldsymbol{\beta}_1}\right\|_2^2/(M-P-PQ+\sum_{i=1}^{PQ}\gamma_{i1}^{-1}\boldsymbol{\Sigma}_{\boldsymbol{\beta}_1}^{ii})\\ \gamma_{i2} &\leftarrow \left|\boldsymbol{\mu}_{\boldsymbol{\beta}_2}^i\right|^2/(1-\gamma_{i2}^{-1}\boldsymbol{\Sigma}_{\boldsymbol{\beta}_2}^{ii})\\ \sigma_2^2 &\leftarrow \left\|\mathbf{x}_{\mathrm{b1}}+\mathbf{X}_{\mathrm{b1}}\boldsymbol{\mu}_{\boldsymbol{\beta}_2}\right\|_2^2/(M-P-PQ+\sum_{i=1}^{PQ}\gamma_{i2}^{-1}\boldsymbol{\Sigma}_{\boldsymbol{\beta}_2}^{ii})\end{aligned} \tag{29, 30}$$

As $\boldsymbol{\beta}_1$ and $\boldsymbol{\beta}_2$ are the same in essence and the observations contain the noise with the same variance, it is necessary to make the following constraints,

$$\begin{aligned}\gamma_i &\leftarrow (\gamma_{i1}+\gamma_{i2})/2\\ \sigma^2 &\leftarrow (\sigma_1^2+\sigma_2^2)/2\end{aligned} \tag{31}$$

Given the initial values of σ^2 and $\boldsymbol{\Sigma}_0$ (i.e. $\gamma_i, i = 1,\ldots,PQ$), the estimation of $\boldsymbol{\beta}$ can be obtained by computing (26) $\sim$ (31) iteratively, until the stopping condition is satisfied. Benefiting from the sparse constraint, the estimation of $\boldsymbol{\beta}$ is much more robust to the choice of P and Q compared to the traditional LS based method [29]–[34]. Usually, P should be larger than the number of the signal components and increase with the level of the measurement noise [32], and Q can be empirically set larger than ten times of P.

B. THE MICRO DOPPLER FREQUENCIES RECOVERY CORRESPONDING TO THE MISSING DATA WITH MIAA

For the gapped sampled return of the target with multiple scatterers, it is difficult to associate the micro Doppler frequencies of multiple scatterers with complex micro motions among the discontinuous segments [14]. Here we would like to overcome this difficulty by recovering the time-varying coefficients of the missing data from those of the observed data and then estimating the micro Doppler frequencies according to (19) and (20).

When the noise is present, the order of the TVAR model is larger than the number of the signal components, which implies that the TVAR coefficients contain the factors from the poles corresponding to the noise. Hence, we need to reduce the influence of the noise in the TVAR coefficients of the observed data to improve the recovery performance. The poles of the signals and the noise are divided by the subspace methods described in [29]–[31]. The estimated poles of the kth scatterer at the mth sampling time is $\hat{\rho}_k(m)$. Define $d_k(m)$ to be the expanded coefficient of the kth order term of the

characterize polynomial $\prod_{k=1}^{K}\left[1-\hat{\rho}_k(m)\,z^{-1}\right]$, i.e.,

$$1+\sum_{k=1}^{K} d_k(m) z^{-k}=\prod_{k=1}^{K}\left[1-\hat{\rho}_k(m)\,z^{-1}\right] \quad m\in\{\text{Observed instants}\} \tag{32}$$

Since the time-varying coefficients of the TVAR model are the linear combination of some basis functions, the missing data recovery approaches for linear model signals can be used to recover $d_k(m)$ corresponding to the missing data. Here, we will adopt the nonparametric MIAA due to its robustness to the noise and the prior information of the signals [16]. Define the column $\mathbf{x}^{\mathrm{o}}$ composed of the estimated TVAR coefficients corresponding to the observed data, the column vectors $\mathbf{d}_k^{\mathrm{o}}$ and $\mathbf{d}_k^{\mathrm{m}}$ composed of $d_k(m)$ corresponding to the observed data and the missing data, respectively, and the column vectors $\mathbf{f}_q^{\mathrm{o}}$ and $\mathbf{f}_q^{\mathrm{m}}$ composed of the elements of $f_q(m)$ corresponding to the sample time of the measured data and missing data, respectively. Then, the expansion coefficients $\alpha_{k,q}$ of $d_k(m)$ and the matrix $\mathbf{R}_k^o$ can be estimated iteratively as follows,

$$\mathbf{R}_k^{\mathrm{o}}=\sum_{q=1}^{Q}|\alpha_{k,q}|\mathbf{f}_q^{\mathrm{o}}\left(\mathbf{f}_q^{\mathrm{o}}\right)^H \tag{33}$$

$$\alpha_{k,q}=\frac{\left(\mathbf{f}_q^{\mathrm{o}}\right)^H\left(\mathbf{R}_k^{\mathrm{o}}\right)^{-1}\mathbf{x}^{\mathrm{o}}}{\left(\mathbf{f}_q^{\mathrm{o}}\right)^H\left(\mathbf{R}_k^{\mathrm{o}}\right)^{-1}\mathbf{f}_q^{\mathrm{o}}} \tag{34}$$

and then recover $\mathbf{d}_k^{\mathrm{m}}$ as,

$$\mathbf{d}_k^{\mathrm{m}}=\sum_{q=1}^{Q}|\alpha_{k,q}|^2\mathbf{f}_q^{\mathrm{m}}\left(\mathbf{f}_q^{\mathrm{m}}\right)^H\left(\mathbf{R}_k^{\mathrm{o}}\right)^{-1}\mathbf{d}_k^{\mathrm{o}} \tag{35}$$

Once the time-varying coefficients $d_k(m)$, $k=1,\cdots,K$, $m\in\{\text{All instants}\}$ are obtained, the poles of the signal components can be computed according to (32) followed by estimating the micro Doppler frequencies according to (20).

C. COMPUTATION COMPLEXITY

The implementation of the proposed method includes three primary steps, and their computation complexities are analyzed as following.

From (13) $\sim$ (16), it is easy to find that the number of the rows and the columns of the forward and backward partially data matrix are $\sum_{g=1}^{G}\left(M_g-P\right)$ and PQ, respectively. Thus, the computation complexity of constructing the forward and backward data matrix is given by,

$$O\left(2PQ\sum_{g=1}^{G}\left(M_g-P\right)\right)$$

According to [35], the computation complexity of each iteration of the SBL algorithm is $O\left(N_{row}^2N_{col}\right)$, where N_{row} and N_{col} are the number of the rows and columns of the dictionary matrix. Considering that the forward and backward coefficient vectors are estimated independently, then the computation complexity of the coefficient vector of the FBTVAR model estimation is given by,

$$O\left(2I_{SBL}\left(\sum_{g=1}^{G}\left(M_g-P\right)\right)^2PQ\right)$$

where I_{SBL} is the iteration number of the SBL algorithm in our method.

Taking advantage of the block Toeplitz structure of the covariance matrix of the gapped sampled data, the iterations of MIAA in (33) and (34) can be computed efficiently [17], and the computation complexity of the MIAA used in our method is given by,

$$KI_{MIAA}O\left(1.5\left(2G-1\right)\left(\sum_{g=1}^{G}M_g\right)^2+12\left(2G-1\right)^3\phi\left(2M_g^{\max}\right)+3\phi\left(PQ\right)\right)$$

where K is the number of the scatterers, I_{MIAA} is the iterative times of the MIAA, $M_g^{\max}$ is the maximum value of M_g, $g=1,\cdots,G$, and $\phi(N)$ denotes the computation complexity of the fast Fourier transform with the matrix size being N.

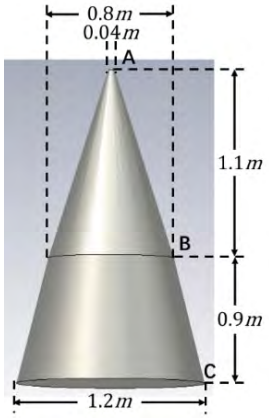

FIGURE 2. The target model.

V. SIMULATIONS AND RESULT ANALYSIS

In this section, we will verify the performance of the proposed approach in recovering the micro Doppler frequencies from the discontinuous radar measurements via several simulations. The radar observations are generated by the professional 3D electromagnetic analysis software CST Studio Suite 2017. The precession-with-nutation object model is a combination of two frustums, as illustrated in Fig.2. The top radius and the base radius of the upper frustum of the cone are 0.04 m and 0.8 m, respectively, and the height is 1.1 m. The top radius and the base radius of the lower frustum of the

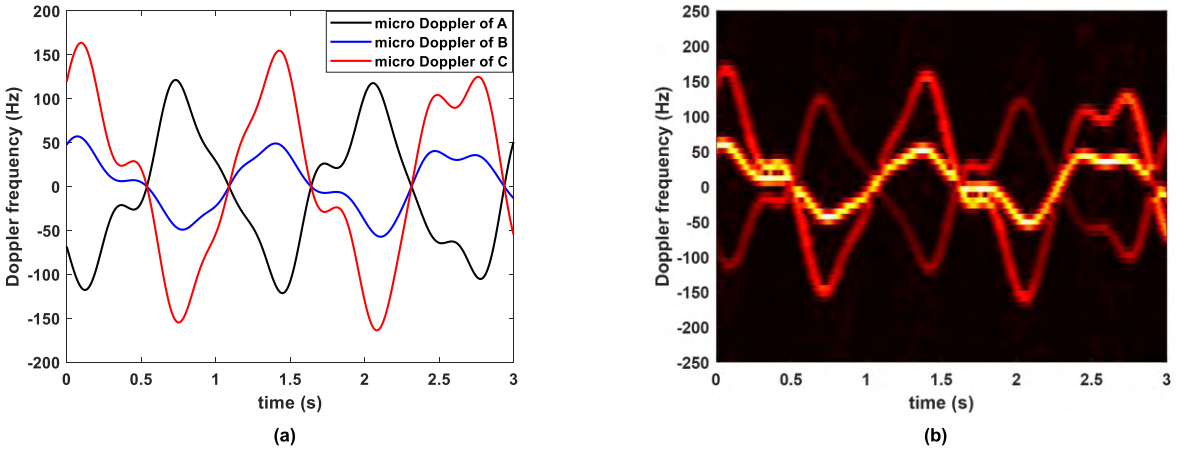

FIGURE 3. The micro Doppler of the spin stabilized target. (a) The micro Doppler of the spin stabilized target computed according to (5). (b) the spectrogram of the micro Doppler signature obtained via STFT.

cone are 0.8 m and 1.2 m, respectively, and the height is 0.9 m. The angular frequencies of the spin, nutation and precession are $\omega_S = 10\pi \text{rad/s}$, $\omega_N = 6\pi \text{rad/s}$ and $\omega_P = 1.6\pi \text{rad/s}$, respectively. The angle between the spin axis and the nutation axis is $\psi = 2°$, the angle between the nutation axis and the precession axis is $\beta = 20°$, and the angle between the LOS axis and the precession axis is $\gamma = 45°$. The center frequency of the radar transmitted signal is $f_c = 10\text{GHz}$, and the pulse repetition frequency is $PRF = 500$ Hz. Fig.2 demonstrates that there are three slipping scatterers on the object of interest that appear to slip around the object as it rotates. They are at the edge of the top of the upper frustum, denoted as A, the edge of the joint between the two frustums and the edge of the bottom of the lower frustum denoted as B and C, respectively.

The micro Doppler of the target model with the micro motion parameters mentioned above is computed according to (5) and illustrated in Fig.3(a). The spectrogram of the micro Doppler signature of the target from the continuous observations is illustrated in Fig.3(b), which is obtained via the short time Fourier transform (STFT) with the rectangular window of 64 points length and 63 overlapped points.

The sparse FBTVAR model parameters are set as $P = 12$, $Q = 200$ and $f_q(m)$ is the Fourier basis function. The signal to noise ratio (SNR) is defined as the ratio of the average power of the target return signal of one pulse to the variance of the white Gaussian noise. We assume that the complete observation interval is 3s and divided into 50 segments with each segment containing 30 samples. The observable segments are selected from the 50 segments randomly with a given proportion. In the other word, the length of the interval of the radar beam dwelling on the target one time is 60ms, which contains the returns of 30 pulses, and the revisit time of the radar for the target is random but is the integer multiple of 60ms.

The iteration of the extended SBL algorithm is stopped once one of the following three conditions is satisfied [35]: the minimum of γ_i is smaller than 10^{-6}, the maximum absolute value of the increment of the elements of $\boldsymbol{\beta}$ between two iterations is smaller than 10^{-6}, and the number of the iterations equals to 500.

The time-frequency map can be obtained from the result of the estimations of the poles and the amplitudes of the TVAR model by

$$\text{TF}(m,f) = \frac{1}{1 + \sum_{k=1}^{3} d_k(m)\, e^{-j\frac{2\pi fk}{PRF}}} \tag{36}$$

where m is the discrete time variable, f is the discrete frequency variable, $d_k(m)$ is the estimation of the time-varying coefficients of the TVAR model.

To further demonstrate the effectiveness of the proposed GSBL-FBTVAR method, some comparisons with the available methods are given in the following simulations. As we have discussed in Section I, there are two relatively latest literatures [27], [28] that handle the problem of the instantaneous frequency recovery from the gapped sampled data of a multicomponent nonstationary signal, and MI-SR (AOK) method is the latest one. In [28], the performance and computation complexity of the MI-SR (AOK) method is compared with the method based on MIAA in the IAF proposed in [27] with shorter signals, which shows that the performance of MI-SR (AOK) is better than MIAA in IAF with much smaller computation loads. Another fact to be noted is that the method of MIAA in the IAF implements the MIAA for every time variable of the IAF, and is impractical in the situation of longer data records due to its large computation workloads requirement [16], [17]. Hence, the MI-SR (AOK) method is chosen to compare with the proposed GSBL-FBTVAR followed by MIAA method.

Furthermore, we also give the results of the LS-FBTVAR method in order to show the benefit of the sparse constraint on the TVAR model in our method, where the traditional LS method is used to estimate the parameters of the TVAR model

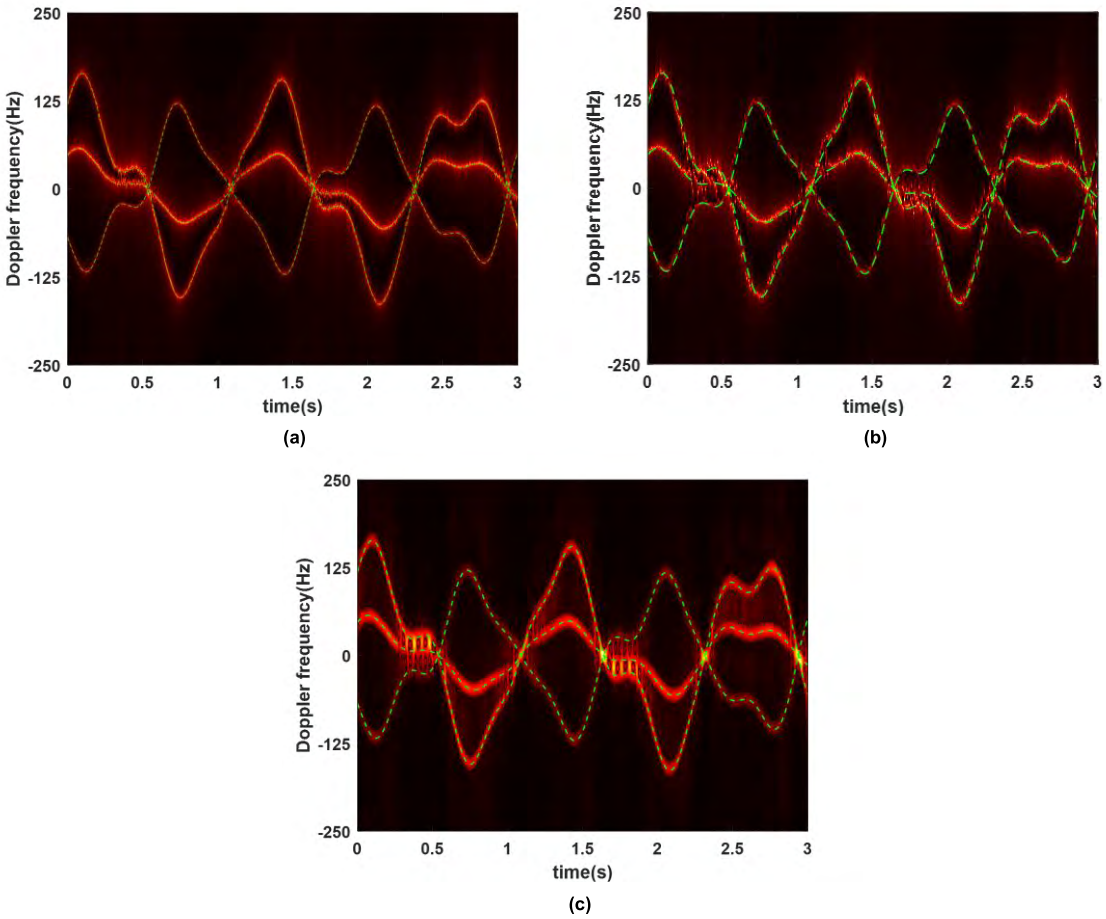

FIGURE 4. The time-frequency maps when the available data is complete and SNR = 25dB obtained by (a) the proposed GSBL-FBTVAR method, (b) the LS-FBTVAR method, and (c) the AOK smoothed WVD, respectively. The dash lines are the ground truth of the micro Dopplers.

according to (17), and the MIAA is used to recover the TVAR model coefficients of the missing data.

A. THE TIME-FREQUENCY MAPS WHEN THE AVAILABLE DATA IS COMPLETE AND SNR = 25dB

Firstly, we would like to investigate the time-frequency resolution of the proposed GSBL-FBTVAR method when the observable data is complete, whose result is compared with that of the LS-FBTVAR method and the AOK smoothed WVD method. To be noted, the MI-SR (AOK) method in [28] degenerates to be the AOK smoothed WVD method [36] when the observation is complete.

Fig.4 shows the time-frequency maps obtained by the three methods when the observable data is complete and the SNR is 25dB. From Fig.4, we can find that the result of the LS-FBTVAR method suffers from the effect of the noise seriously, and the time-frequency resolution is worse in the vicinity of the cross points of the micro Doppler frequencies of different scatterers. The result of the AOK smoothed WVD method is affected by the noise to a lesser degree, but it cannot resolve different micro Doppler frequency components completely when they are close to each other. The proposed GSBL-FBTVAR method can still work well, which gives the time-frequency map with much better time-frequency aggregativeness and higher time-frequency resolution simultaneously.

B. THE TIME-FREQUENCY MAPS VERSUS DIFFERENT PROPORTIONS OF THE AVAILABLE SAMPLES WHEN SNR = 20dB

In this subsection, we will analyze the performance of the proposed GSBL-FBTVAR method when the data is gapped sampled with different proportions of the available samples at a relatively high SNR setting. The results are also compared with those of the MI-SR (AOK) and the LS-FBTVAR methods.

Fig.5 $\sim$ Fig.6 illustrate the recovery results of the micro Doppler via the GSBL-FBTVAR, the LS-FBTVAR, and the MI-SR (AOK) method, when the proportions of the available samples to the complete signal are 20% and 50%, respectively and the SNR is 20dB. From Fig.5 $\sim$ Fig.6, we can find that the accuracy of the recovery results is greatly improved with the increasing proportion of the available samples. Under the condition that the proportion of

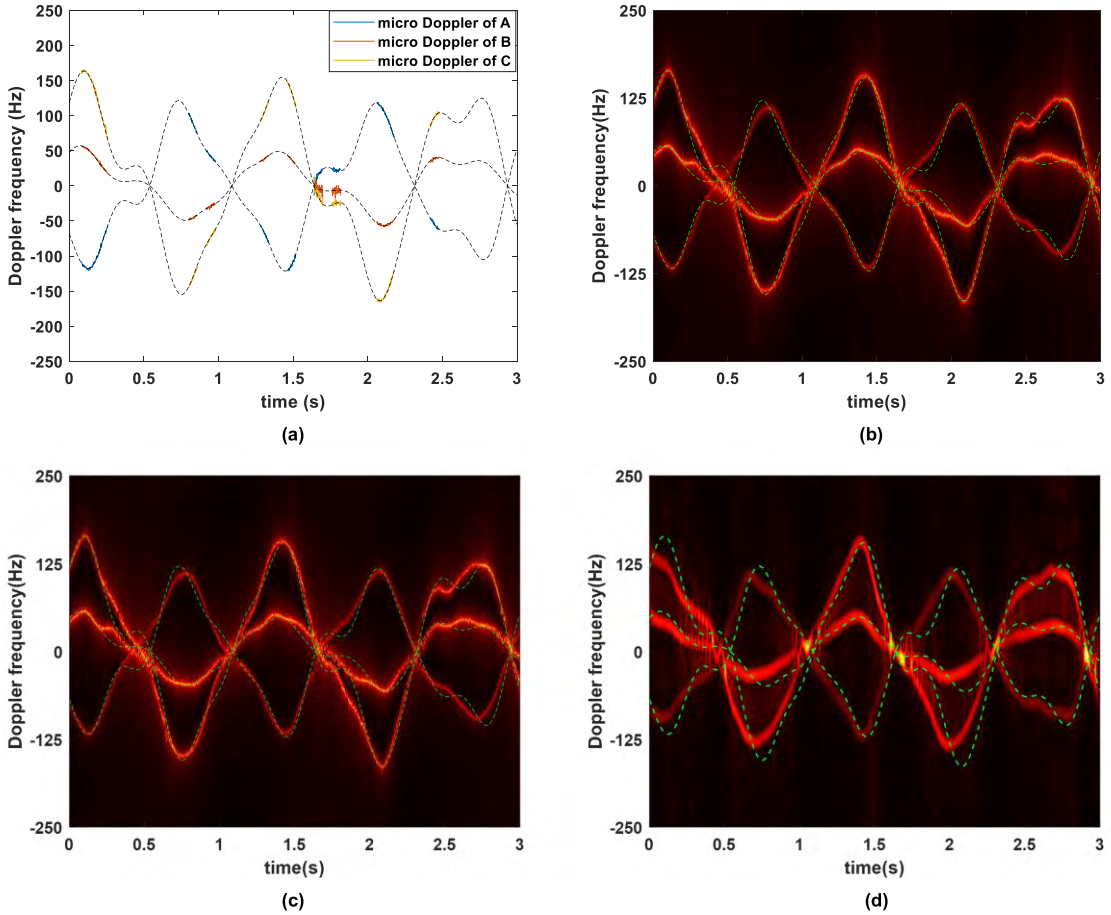

FIGURE 5. The recovery results of the micro Doppler when the proportion of the available samples is 20% and SNR = 20dB. (a) The micro Doppler frequencies estimated by the GSBL-FBTVAR. (b) the time-frequency map generated from the estimations obtained by the GSBL-FBTVAR followed by MIAA. (c) The time-frequency map generated from the estimations obtained by the LS-FBTVAR followed by MIAA. (d) The time-frequency map generated by the MI-SR (AOK) method. The dash lines are the ground truth of the micro Dopplers.

the available samples is 20%, there exist relative more parts that the recovered micro Doppler frequencies deviate their real values obviously. When the proportion of the available samples reaches 50%, the recovered micro Dopplers frequencies are quite close to the truths. Compared with the results obtained by the GSBL-FBTVAR, the recovered results of the MI-SR (AOK) method lead to much larger deviation from the real values of the micro Doppler frequencies. We can also find that there exists obvious overfitting phenomenon in the results of the LS-FBTVAR, and the reason is that the LS technology is used directly for gapped sampled data without any regularization constraints.

C. THE TIME-FREQUENCY MAPS VERSUS DIFFERENT PROPORTIONS OF THE AVAILABLE SAMPLES WHEN SNR = 0dB

In this subsection, we will validate the performance of the proposed GSBL-FBTVAR method versus different proportions of the available samples with a relatively low SNR setting.

The recovery results of the micro Doppler are demonstrated in Fig.7 $\sim$ Fig.8, when the proportions of the available samples to the complete signal are 20% and 50%, respectively and the SNR is 0dB. From Fig.7 $\sim$ Fig.8, it is obvious that the proposed method is more robust than the LS-FBTVAR method and the MI-SR (AOK) method in the lower SNR situation. Considering that the definition of the SNR is the average power of the returns to the variance of the noise and there are three scatterers, the SNR of each scatterer is actually lower than 0dB. In such a lower SNR condition, the proposed method can still work with a satisfactory accuracy, though the variances of the recovered results are relative larger. However, the MI-SR (AOK) method is affected by the noise too seriously to identify the micro Doppler frequencies of different scatterers. The LS-FBTVAR method can give distinct micro Doppler spectrum under the low SNR condition, but it suffers from serious overfitting, especially when the proportion of the missing data is larger.

To be noted, it is usually hard to associate the micro Dopplers of multiple scatterers among the discontinuous

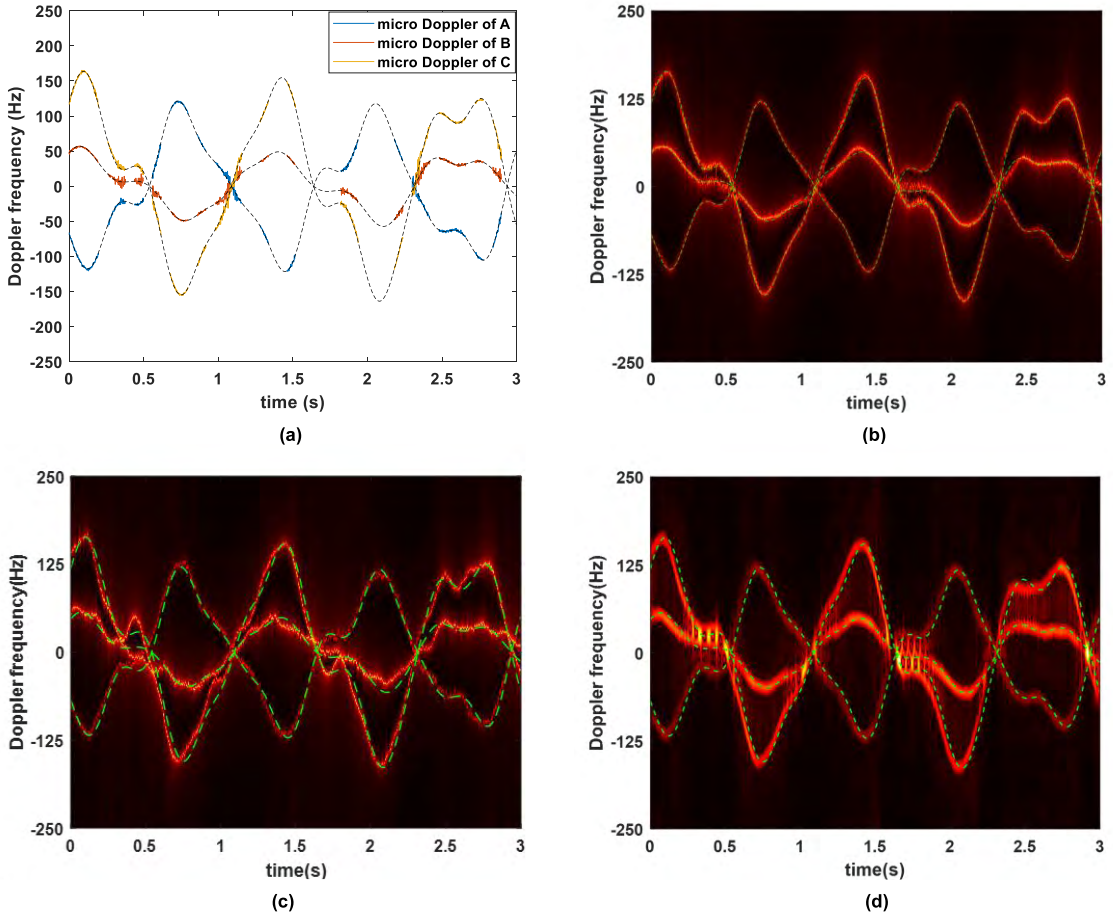

FIGURE 6. The recovery results of the micro Doppler when the proportion of the available samples is 50% and SNR = 20dB. (a) The micro Doppler frequencies estimated by the GSBL-FBTVAR. (b) The time-frequency map generated from the estimations obtained by the GSBL-FBTVAR followed by MIAA. (c) The time-frequency map generated from the estimations obtained by the LS-FBTVAR followed by MIAA. (d) The time-frequency map generated by the MI-SR (AOK) method. The dash lines are the ground truth of the micro Dopplers.

observation segments in Fig.7(a) $\sim$ Fig.8(a). While the difficulty of the association can be avoided by transferring the problem of recovering instantaneous frequencies of the multiple components into recovering the coefficients of the TVAR model as described in subsection 4.2. That is, the proposed GSBL-FBTVAR method does not involve the association problem.

D. THE PERFORMANCE ASSESMENT OF THE DOPPLER FREQUENCY RECOVERY

In order to evaluate the performance of the proposed micro Doppler frequency recovery method quantitatively, we calculate the root mean square error (RMSE) of the recovered Doppler frequencies with 100 independent trials. Fig.9(a) illustrates the RMSE curves of the recovered Doppler frequencies as a function of the observable proportion (OP) under different SNRs and Fig.9(b) illustrates the RMSE as a function of the SNR corresponding to different observable proportions.

From Fig.9, we can find that the RMSE of the recovery decreases with the increasing SNR and the proportion of the available samples. According to the curves showed in Fig.9, it is observable that when the proportion of the observable data is less than 0.4, the RMSE of the recovered micro Doppler frequencies decreases with the increasing proportions of the available data distinctly; in contrast, when the observable proportion is larger than 0.4, the decreasing trend of the RMSE versus the observable proportion is much flatter. And this phenomenon is also present under different SNR conditions. Therefore, we can deduce that the confidence level of the results obtained via the proposed method is relatively higher when the proportion of the available data is larger than 40%.

Furthermore, we compare the RMSE of the micro Doppler frequencies recovered by the proposed method, the LS-FBTVAR method and the MI-SR(AOK) method under different available data proportions and SNRs. The RMSEs are evaluated with 100 independent trials and the results are illustrated in Fig.10 and Fig.11. Fig.10 shows the RMSEs of the three methods that vary with the increasing available data

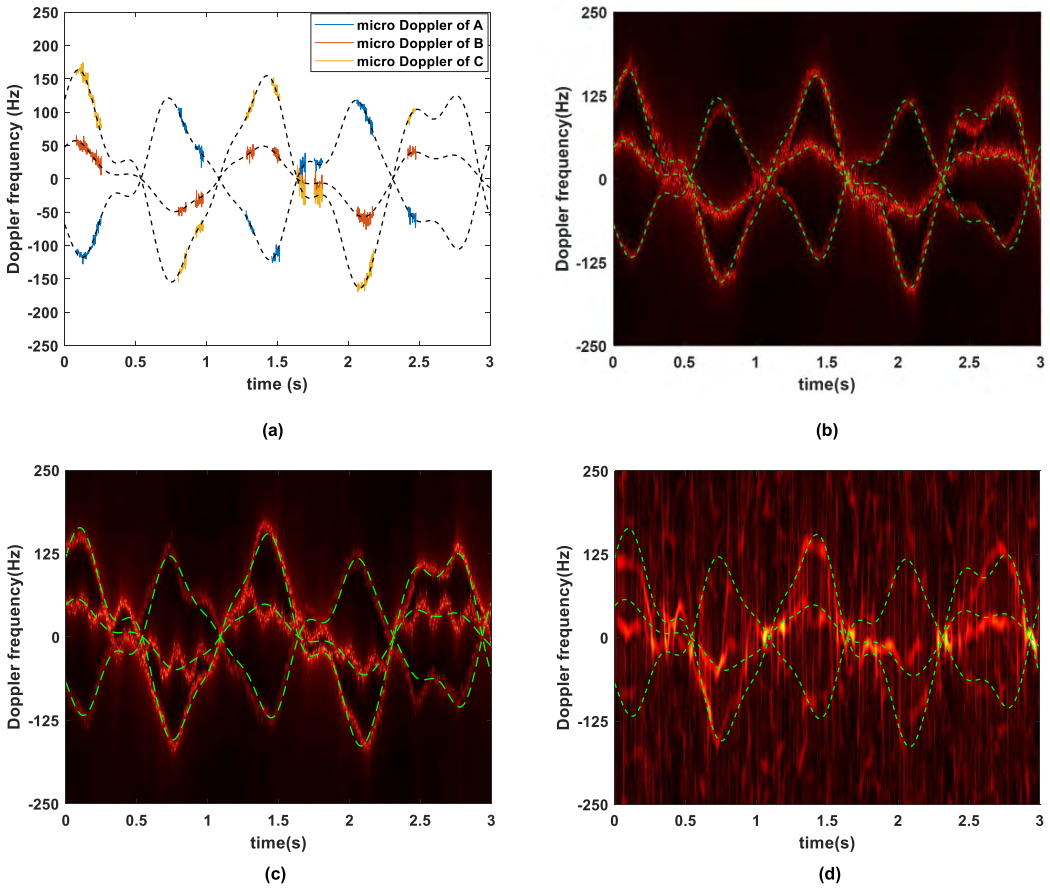

FIGURE 7. The recovery results of the micro Doppler when the proportion of the available samples is 20% and SNR = 0dB. (a) The micro Doppler frequencies estimated by the GSBL-FBTVAR. (b) the time-frequency map generated from the estimations obtained by the GSBL-FBTVAR followed by MIAA. (c) The time-frequency map generated from the estimations obtained by the LS-FBTVAR followed by MIAA. (d) The time-frequency map generated by the MI-SR (AOK) method. The dash lines are the ground truth of the micro Dopplers.

proportions when the SNRs are 5dB, 10dB, 15dB and 20dB, respectively. From Fig.10, we can find that the RMSEs of the micro Doppler frequencies recovered by the three methods decrease as the observable proportion increases. When the OP is small, the performance of the proposed method is much better than that of the MI-SR(AOK) method. And the gap of the RMSEs between the two methods gradually decreases with the increasing OP. The LS-FBTVAR method always gives the worst RMSE because there is no regularization constraint in the model and the overfitting generally occurs especially when the observation is not continuous.

In Fig.11, we demonstrate the RMSEs of the three methods that vary with the increasing SNRs when the available data proportions are 20%, 40%, 60%, and 80%, respectively. Fig.11 illustrates that the performance of the three methods improves as the SNR increases. The curves also reveal that under the same conditions of SNR and observable proportion, the RMSE of the proposed method is the lowest compared with that of the LS-FBTVAR method and the MI-SR(AOK) method. The RMSE of the LS-FBTVAR method does not change obviously. This is because there is no sparse constraint in the FBTVAR model, which may cause serious overfitting and hence large RMSEs. The performance of the MI-SR (AOK) method is much worse than that of the proposed method when the SNR is low, and gradually approaches to that of the proposed method when the SNR becomes higher. The reason is that the MI-SR(AOK) method is a quadratic method and suffers from the interference of the cross terms in low SNR situations [28].

In conclude, both Fig.10 and Fig.11 imply that the proposed GSBL-FBTVAR method has the best performance of recovering the micro-Doppler frequencies.

E. THE COMPUTATION COMPLEXITY OF THE PROPOSED METHOD

In this subsection, we would like to evaluate the computation times of the proposed GSBL-FBTVAR method, the LS-FBTVAR, and the MI-SR(AOK) method. All the simulations are implemented with MATLAB 2018b in the workstation with Intel i7 6700HQ processor (Quad core, 2.6GHz), and the memory is 32GB. The computation times of the three methods are listed in Table 1, and the unit of the time is second.

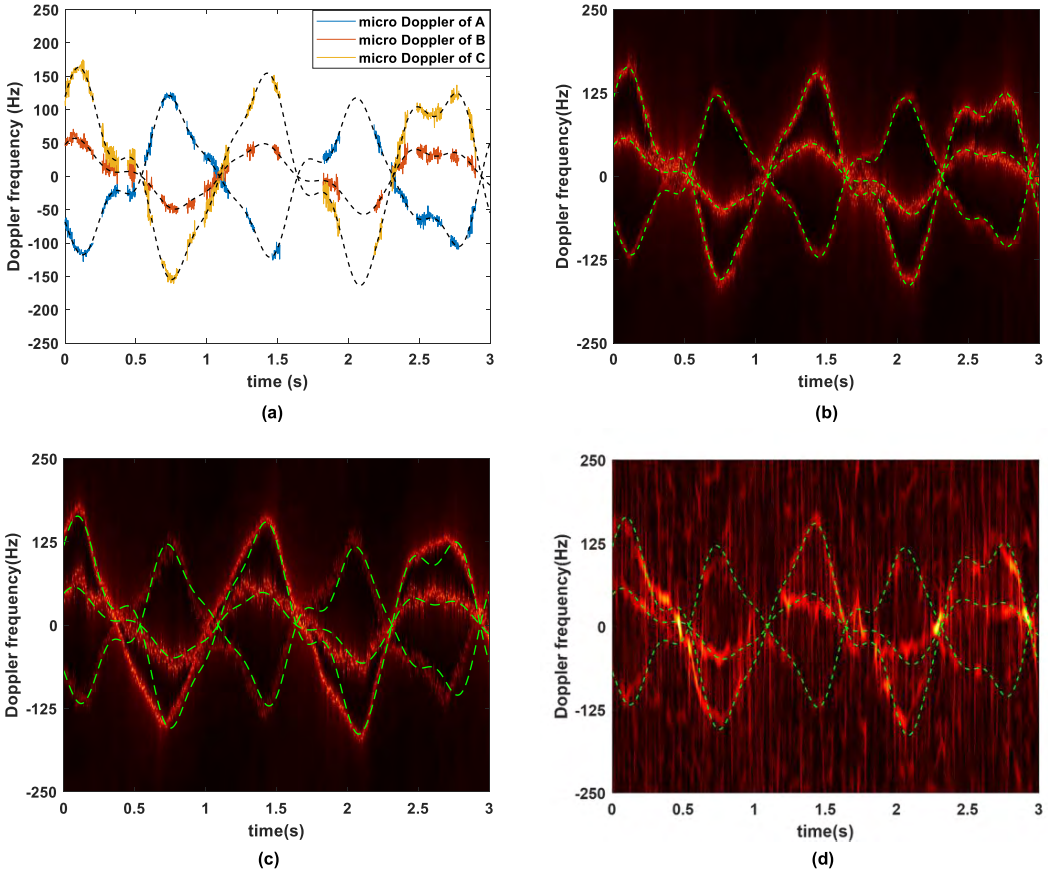

FIGURE 8. The recovery results of the micro Doppler when the proportion of the available samples is 50% and SNR = 0dB. (a) The time-frequency map generated from the estimations obtained by the GSBL-FBTVAR followed by MIAA. (c) The time-frequency map generated from the estimations obtained by the LS-FBTVAR followed by MIAA. (d) The time-frequency map generated by the MI-SR (AOK) method. The dash lines are the ground truth of the micro Dopplers.

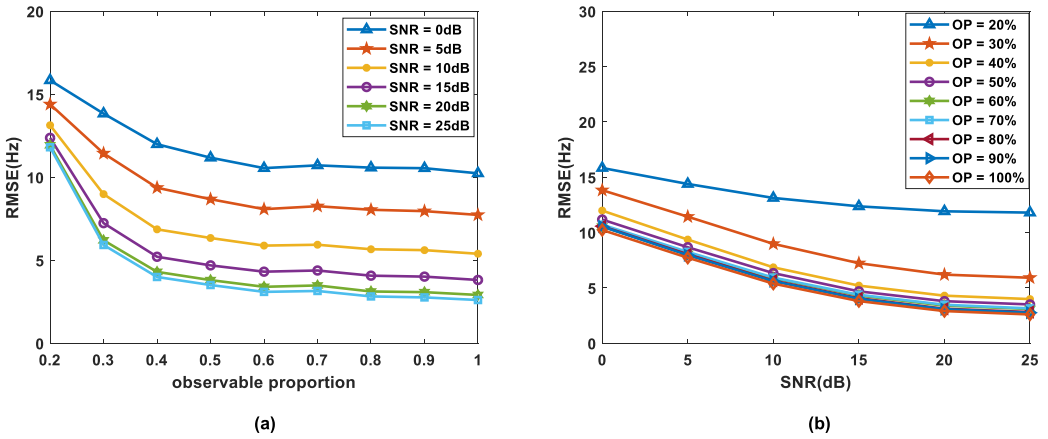

FIGURE 9. (a) The RMSE curves of the recovered micro Doppler frequencies via the proposed method versus the available data proportions when the SNR is varying from 0dB to 25dB. (b) The RMSE curves of the recovered micro Doppler frequencies versus SNRs when the observable proportions are varying from 20% to 100%.

According to (17) and (18), the computation complexities of the GSBL-FBTVAR, the LS-FBTVAR method, and the MIAA method used followed them depend on the number of samples. As a result, we evaluate the computation time of these two methods when the observable proportion is from 20% to 90%. From Table 1, we can find that as the cost of the much better performance, the required computation time of the GSBL-FBTVAR method is much larger than that of the LS-FBTVAR method, and increases distinctly with the increasing observable proportion. According to [28], when the AOK is used in the IAF of the signal, the missing data of the IAF without smoothing is disappeared, and the computation time of the MI-SR (AOK) method does not change with the observable proportion. Since the sparse reconstruction

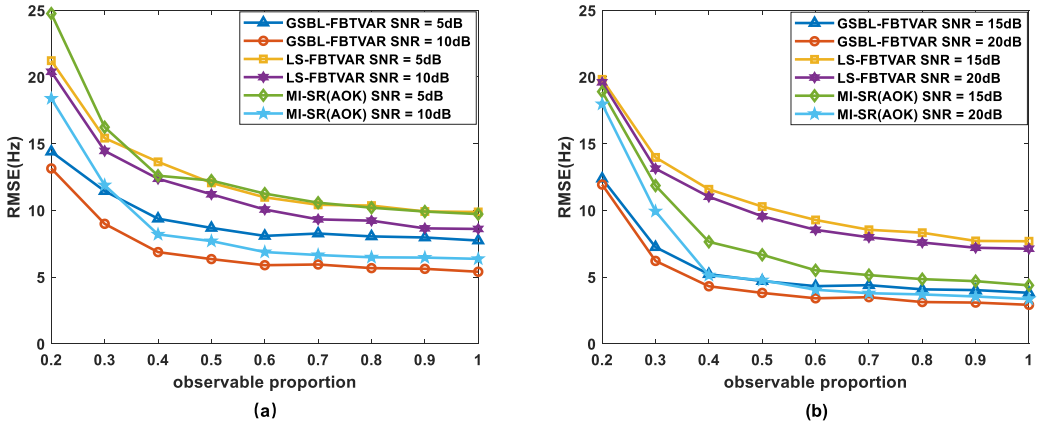

FIGURE 10. (a) The RMSE curves of the recovered micro Doppler frequencies obtained by the proposed method and the two comparative methods versus the available data proportions when the SNRs are 5dB and 10dB, respectively. (b) The RMSE curves of the recovered micro Doppler frequencies obtained by the proposed method and the two comparative methods versus the available data proportions when the SNRs are 15dB and 20dB, respectively.

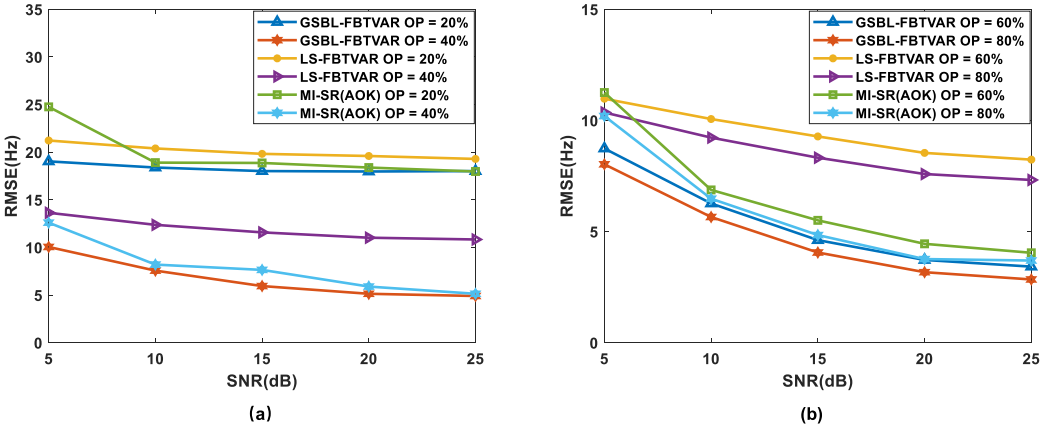

FIGURE 11. (a) The RMSE curves of the recovered micro Doppler frequencies obtained by the proposed method and the two comparative methods versus SNRs when the observable proportions are 20% and 40%, respectively. (b) The RMSE curves of the recovered micro Doppler frequencies obtained by the proposed method and the two comparative methods versus SNR when the observable proportions are 60% and 80%, respectively.

TABLE 1. Computation time comparison of the three methods.

OP	GSBL-FBTVAR(s)	LS-FBTVAR(s)	MI-SR(AOK)(s)
20%	2.5410	0.9949	80.5563
30%	4.8582	1.0167	80.5563
40%	6.4359	1.0518	80.5563
50%	13.1978	1.1139	80.5563
60%	19.2913	1.2017	80.5563
70%	39.3168	1.3354	80.5563
80%	45.5811	1.4646	80.5563
90%	55.1442	1.6221	80.5563

should be implemented with respect to the lag variable for all time variables, the computation time of the MI-SR(AOK) increases linearly with the number of the time variables of the recovered time-frequency map, and is much more than that of the proposed GSBL-TVAR method.

VI. CONCLUSION

To estimate the micro Doppler frequencies of a spin stabilized object from discontinuous observations caused by multiple target tracking or multiple task of the radar, a sparse FBTVAR model based method referred to as GSBL-FBTVAR was proposed in this paper. An extended SBL algorithm was developed to estimate the coefficients of the sparse FBTVAR model from the discontinuous observations and the MIAA algorithm was used to recover the FBTVAR coefficients corresponding to the missing data. The proposed method not only has the ability of instantaneous Doppler estimation from discontinuous observations jointly, but also can effectively avoid the micro Doppler frequencies association of multiple scatterers among the discontinuous observation segments. The simulations demonstrate that the proposed method is more robust compared with the existing method under the conditions of lower SNRs and less available data.

REFERENCES

[1] B. Wie, *Space Vehicle Dynamics and Control*, 2nd Ed. Reston, VA, USA: American Institute of Aeronautics and Astronautics, 2008.
[2] V. C. Chen, D. Tahmoush, and W. J. Miceli, *Radar Micro-Doppler Signatures: Processing and applications*. Edison, NJ, USA: IET, 2014.
[3] V. C. Chen, *The Micro-Doppler Effect in Radar*. Boston, MA, USA: Artech House, 2010.
[4] V. C. Chen, F. Li, S.-S. Ho, and H. Wechsler, "Micro-Doppler effect in radar: Phenomenon, model, and simulation study," *IEEE Trans. Aerosp. Electron. Syst.*, vol. 42, no. 1, pp. 2–21, Jan. 2006.

[5] L. Zhu, S. Zhang, H. Zhao, S. Chen, D. Wei, and X. Lu, "Classification of UAV-to-ground vehicles based on micro-Doppler signatures using singular value decomposition and deep convolutional neural networks," *IEEE Access*, vol. 7, pp. 22133–22143, 2019.
[6] Y. Ding, C. Lei, X. Xu, K. Sun, and L. Wang, "Human micro-Doppler frequency estimation approach for Doppler radar," *IEEE Access*, vol. 6, pp. 6149–6159, 2018.
[7] H. Gao, L. Xie, S. Wen, and Y. Kuang, "Micro-Doppler signature extraction from ballistic target with micro-motions," *IEEE Trans. Aerosp. Electron. Syst.*, vol. 46, no. 4, pp. 1969–1982, Oct. 2010.
[8] X.-Y. Pan, J. Liu, L.-T. Xu, X. Ai, Q. Xie, B. Yu, and C. Li, "Extraction of micro-Doppler frequency from HRRPs of rotating targets," *IEEE Access*, vol. 5, pp. 26162–26174, 2017.
[9] P. Lei, J. Wang, and J. Sun, "Analysis of radar micro-Doppler signatures from rigid targets in space based on inertial parameters," *IET Radar Sonar Navigat.*, vol. 5, no. 2, pp. 93–102, Feb. 2011.
[10] Y. Luo, Q. Zhang, N. Yuan, F. Zhu, and F. Gu, "Three-dimensional precession feature extraction of space targets," *IEEE Trans. Aerosp. Electron. Syst.*, vol. 50, no. 2, pp. 1313–1329, Apr. 2014.
[11] L. Hong, F. Dai, and H. Liu, "Motion-parameter estimation for precession-with-nutation space targets based on wideband radar measurements," *IEEE Trans. Aerosp. Electron. Syst.*, vol. 52, no. 2, pp. 643–657, Apr. 2016.
[12] A. R. Persico, C. Clemente, D. Gaglione, C. V. Ilioudis, J. Cao, L. Pallotta, A. De Maio, I. Proudler, and J. J. Soraghan, "On model, algorithms, and experiment for micro-Doppler-based recognition of ballistic targets," *IEEE Trans. Aerosp. Electron. Syst.*, vol. 53, no. 3, pp. 1088–1108, Jun. 2017.
[13] P. Xia, X. R. Wan, J. X. Yi, and H. Tang, "Micro-Doppler imaging for fast rotating targets using illuminators of opportunity," *IET Radar, Sonar Navigat.*, vol. 10, no. 6, pp. 1024–1029, 2016.
[14] Y. Shi, B. Jiu, and H. Liu, "Optimization-based discontinuous observation strategy for micro-Doppler signature extraction of space cone targets," *IEEE Access*, vol. 7, pp. 58915–58929, 2019.
[15] E. G. Larsson, P. Stoica, and J. Li, "Amplitude spectrum estimation for two-dimensional gapped data," *IEEE Trans. Signal Process.*, vol. 50, no. 6, pp. 1343–1354, Jun. 2002.
[16] P. Stoica, J. Li, and J. Ling, "Missing data recovery via a nonparametric iterative adaptive approach," *IEEE Signal Process. Lett.*, vol. 16, no. 4, pp. 241–244, Apr. 2009.
[17] G.-O. Glentis and A. Jakobsson, "Efficient implementation of iterative adaptive approach spectral estimation techniques," *IEEE Trans. Signal Process.*, vol. 59, no. 9, pp. 4154–4167, Sep. 2011.
[18] M. Elad, *Sparse and Redundant Representations: From Theory to Applications in Signal and Image Processing*. Springer, 2010.
[19] B. Jokanovic and M. Amin, "Reduced interference sparse time-frequency distributions for compressed observations," *IEEE Trans. Signal Process.*, vol. 63, no. 24, pp. 6698–6709, Dec. 2015.
[20] L. Stanković, S. Stanković, I. Orović, and Y. D. Zhang, *Time–Frequency Analysis of Micro-Doppler Signals Based on Compressive Sensing* (Compressive Sensing for Urban Radars), S. Amin Ed. Boca Raton, FL, USA: CRC Press, 2014, pp. 283–326.
[21] I. Stanković, C. Ioana, and M. Daković, "On the reconstruction of non-sparse time-frequency signals with sparsity constraint from a reduced set of samples," *Signal Process.*, vol. 142, pp. 480–484, Jan. 2018.
[22] E. Sejdić, I. Orović, and S. Stanković, "Compressive sensing meets time–frequency: An overview of recent advances in time–frequency processing of sparse signals," *Digit. Signal Process.*, vol. 77, pp. 22–35, Jun. 2018.
[23] P. Flandrin and P. Borgnat, "Time-frequency energy distributions meet compressed sensing," *IEEE Trans. Signal Process.*, vol. 58, no. 6, pp. 2974–2982, Jun. 2010.
[24] M. G. Amin, B. Jokanovic, Y. D. Zhang, and F. Ahmad, "A sparsity-perspective to quadratic time–frequency distributions," *Digit. Signal Process.*, vol. 46, pp. 175–190, Nov. 2015.
[25] N. A. Khan and S. Ali, "Sparsity-aware adaptive directional time–frequency distribution for source localization," *Circuits, Syst., Signal Process.*, vol. 37, no. 3, pp. 1223–1242, Mar. 2018.
[26] L. Stanković, I. Orović, S. Stanković, and M. Amin, "Compressive sensing based separation of nonstationary and stationary signals overlapping in time-frequency," *IEEE Trans. Signal Process.*, vol. 61, no. 18, pp. 4562–4572, Sep. 2013.
[27] Y. D. Zhang, "Resilient quadratic time-frequency distribution for FM signals with gapped missing data," in *Proc. IEEE Radar Conf. (RadarConf)*, Seattle, WA, USA, May 2017, pp. 1765–1769.
[28] V. S. Amin, Y. D. Zhang, and B. Himed, "Sparsity-based time-frequency representation of FM signals with burst missing samples," *Signal Process.*, vol. 155, pp. 25–43, Feb. 2019.
[29] Y. Grenier, "Time-dependent ARMA modeling of nonstationary signals," *IEEE Trans. Acoust., Speech, Signal Process.*, vol. ASSP-31, no. 4, pp. 899–911, Aug. 1983.
[30] A. A. Beex and P. Shan, "A time-varying Prony method for instantaneous frequency estimation at low SNR," in *Proc. IEEE Int. Symp. Circuits Syst. VLSI*, vol. 3, Orlando, FL, USA, May/Jun. 1999, pp. 5–8.
[31] S. Mukhopadhyay and P. Sircar, "Parametric modelling of non-stationary signals: A unified approach," *Signal Process.*, vol. 60, no. 2, pp. 135–152, Jul. 1997.
[32] A. T. Johansson and P. R. White, "Instantaneous frequency estimation at low signal-to-noise ratios using time-varying notch filters," *Signal Process.*, vol. 88, no. 5, pp. 1271–1288, May 2008.
[33] M. Jachan, G. Matz, and F. Hlawatsch, "Time-frequency ARMA models and parameter estimators for underspread nonstationary random processes," *IEEE Trans. Signal Process.*, vol. 55, no. 9, pp. 4366–4381, Sep. 2007.
[34] H. Ijima and E. Grivel, "Deterministic regression methods for unbiased estimation of time-varying autoregressive parameters from noisy observations," *Signal Process.*, vol. 92, no. 4, pp. 857–871, Apr. 2012.
[35] D. P. Wipf and B. D. Rao, "An empirical Bayesian strategy for solving the simultaneous sparse approximation problem," *IEEE Trans. Signal Process.*, vol. 55, no. 7, pp. 3704–3716, Jul. 2007.
[36] D. L. Jones and R. G. Baraniuk, "An adaptive optimal-kernel time-frequency representation," *IEEE Trans. Signal Process.*, vol. 43, no. 10, pp. 2361–2371, Oct. 1995.

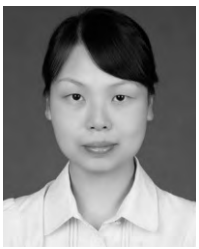

LING HONG received the B.S. and Ph.D. degrees in electronic engineering from Xidian University, Xi'an, China, in 2008 and 2015, respectively. She is currently an Associate Researcher with the School of Computer Science, Shaanxi Normal University, Xi'an. Her research interests include radar signal processing and intelligent information processing.

FENGZHOU DAI received the B.S., M.S., and Ph.D. degrees in electronic engineering from Xidian University, Xi'an, China, in 2002, 2005, and 2010, respectively, where he is currently an Associate Professor with the National Laboratory of Radar Signal Processing. His research interests include radar signal processing and microwave imaging.

XILI WANG received the B.S. degree in computer science from Tianjin University, Tianjin, China, in 1991, and the M.S. and Ph.D. degrees in computer science and electronic engineering from Xidian University, Xi'an, China, in 1994 and 2004, respectively. She is currently a Professor with the School of Computer Science, Shaanxi Normal University. Her research interests include intelligent information processing and image perception and understanding.